Supplementary Information

Stabilized Cu^0-Cu^{1+} Dual Sites in a Cyanamide Framework for Selective CO_2 Electroreduction to Ethylene

Kaihang Yue [1,2,6], Yanyang Qin [3,6], Honghao Huang [1], Zhuoran Lv [1,4], Mingzhi Cai [4,5], Yaqiong Su [3]*, Fuqiang Huang [1,4,]*, and Ya Yan [1,2,]*

[1] State Key Laboratory of High Performance Ceramics and Superfine Microstructure, Shanghai Institute of Ceramics, Chinese Academy of Sciences, Shanghai 200050, China.

[2] Center of Materials Science and Optoelectronics Engineering, University of Chinese Academy of Sciences, Beijing 100049, China.

[3] School of Chemistry, Xi'an Jiaotong University, Xi'an 710049, China

[4] State Key Lab of Metal Matrix Composites, School of Materials Science and Engineering, Shanghai Jiao Tong University, Shanghai 200240, China

[5] State Key Laboratory of Rare Earth Materials Chemistry and Applications College of Chemistry and Molecular Engineering, Peking University, Beijing 100871, China

[6] These authors contributed equally: Kaihang Yue, Yanyang Qin.

Corresponding author E-mail: yqsu1989@xjtu.edu.cn (YQS), huangfq@sjtu.edu.cn (FQH), yanya@mail.sic.ac.cn (YY)

Supplementary Figures

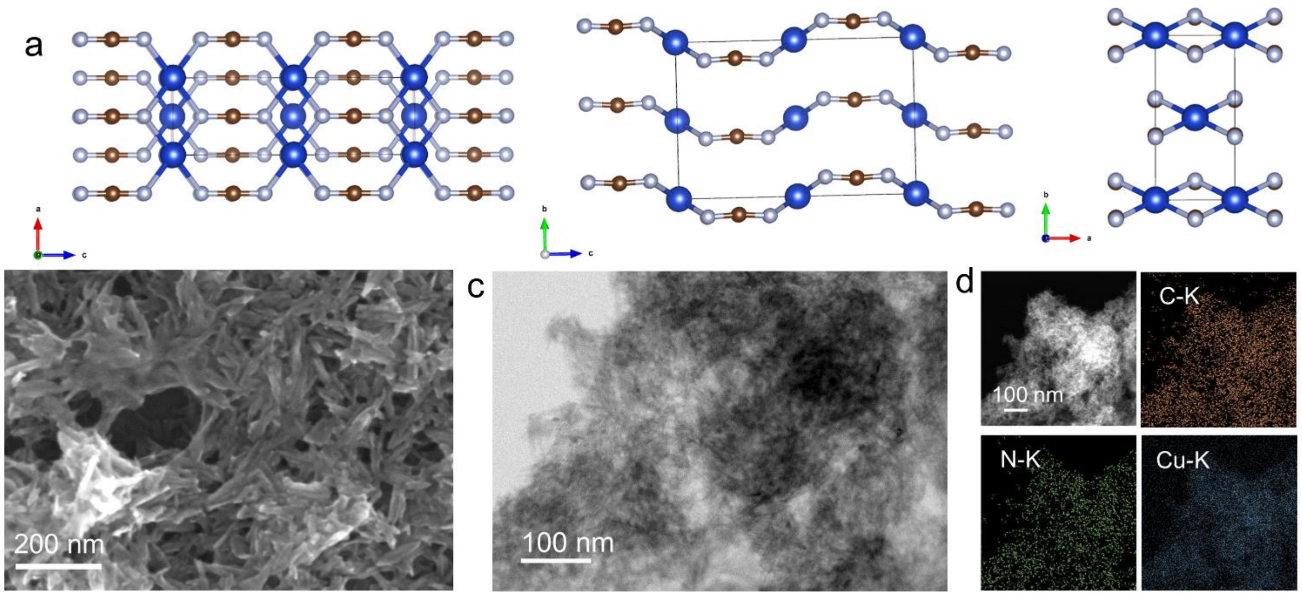

Supplementary Fig. 1. The structural model and electron microscopy images of CuNCN. (a) Crystal structure of CuNCN. (b) SEM, (c) TEM image of CuNCN. (d) EDS mapping of CuNCN.

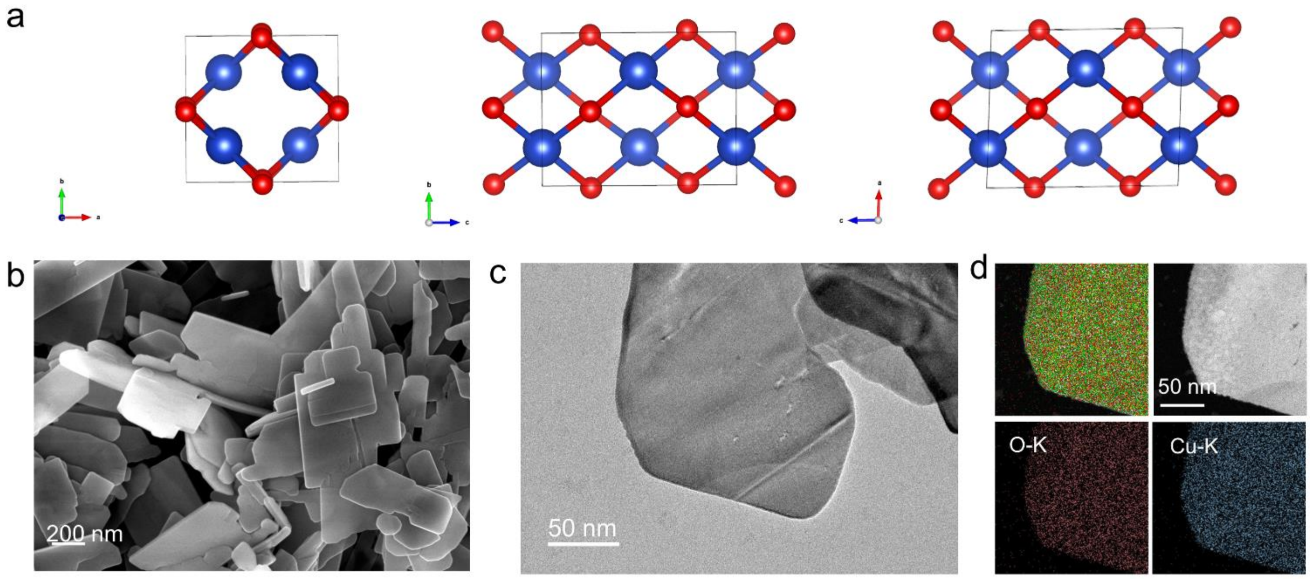

Supplementary Fig. 2. The structural model and electron microscopy images of CuO. (a) Crystal structure of CuO. (b) SEM, (c) TEM image of CuO. (d) EDS mapping of CuO.

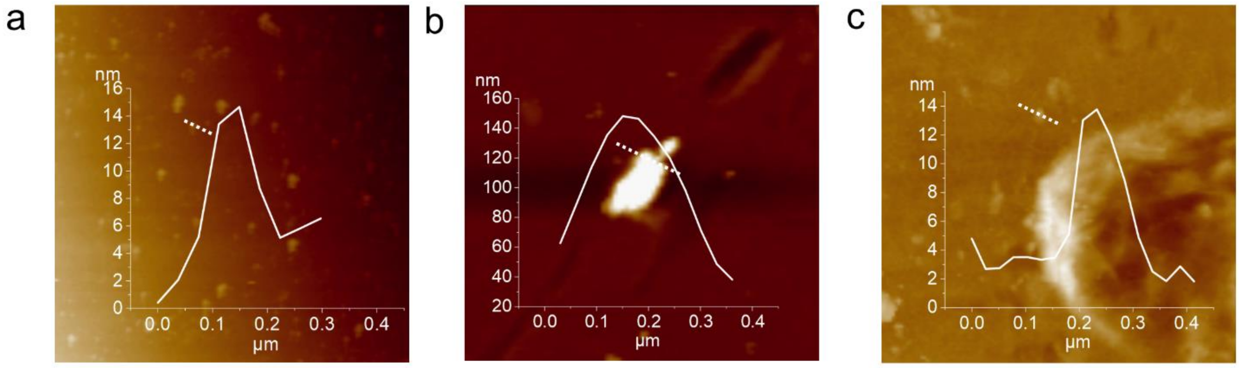

Supplementary Fig. 3. AFM image of (a) $Cu^{\delta+}$NCN, (b) CuNCN and (c) CuO.

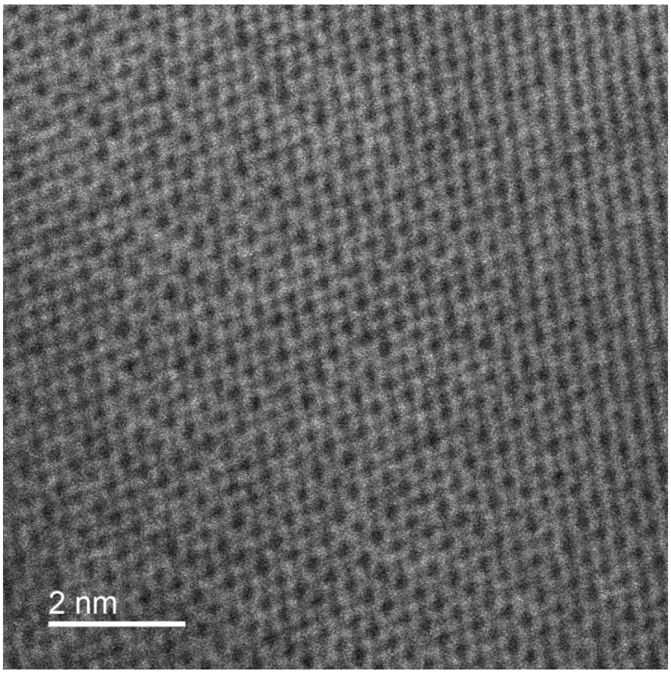

Supplementary Fig. 4. ABF image of $Cu^{\delta+}$NCN in STEM.

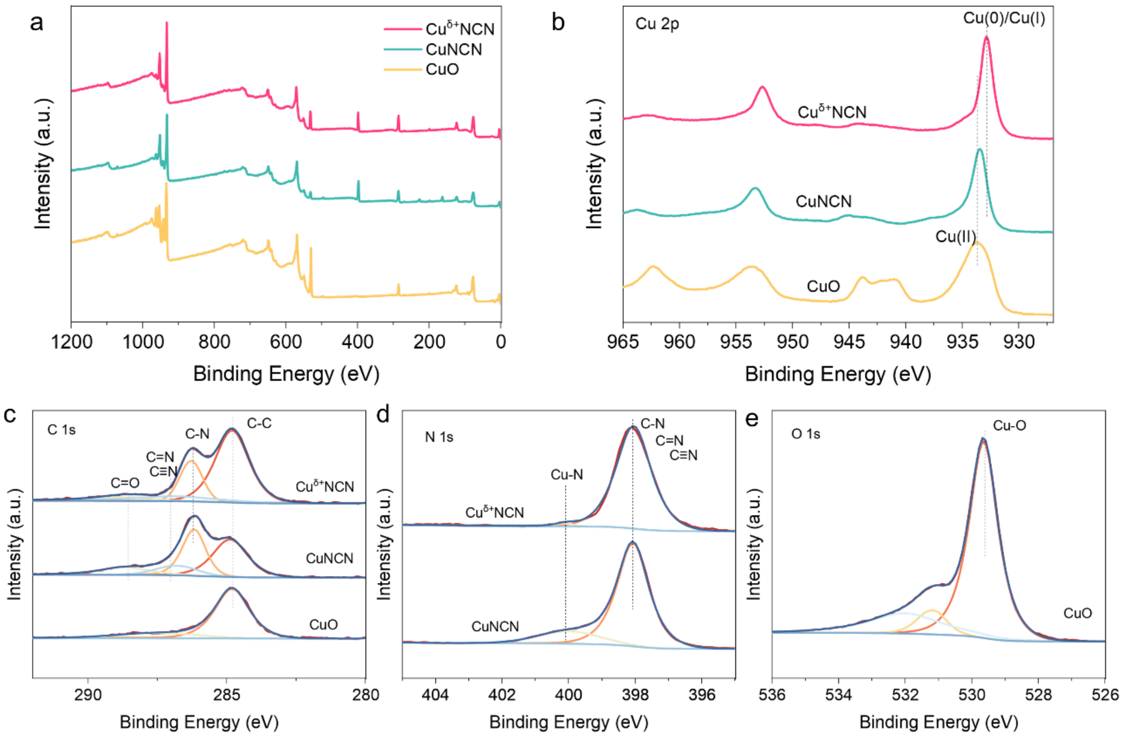

Supplementary Fig. 5. XPS spectra of Cu$^{\delta+}$NCN, CuNCN and CuO. (a) XPS survey spectra. (b) Cu 2p, (c) C 1s high-resolution XPS of Cu$^{\delta+}$NCN, CuNCN and CuO. (d) N 1s high-resolution XPS of Cu$^{\delta+}$NCN and CuNCN. (e) O 1s high-resolution XPS of CuO.

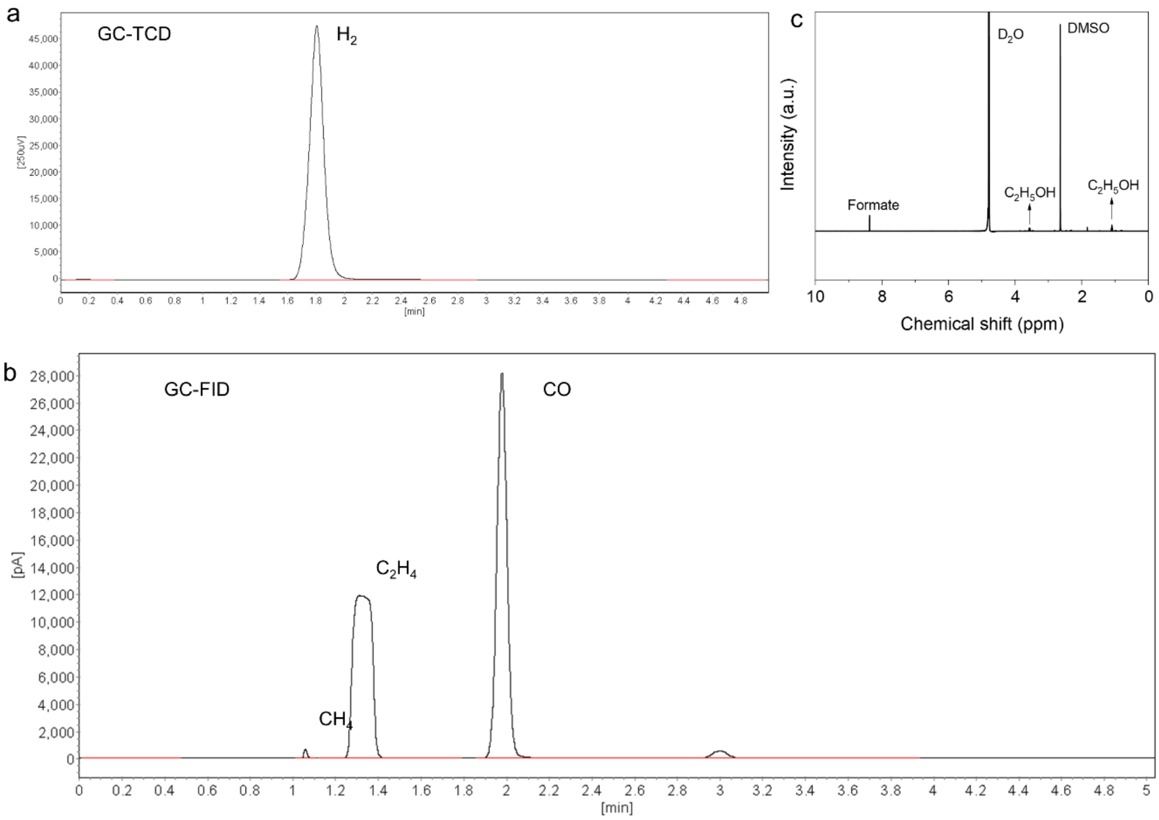

Supplementary Fig. 6. Representative data on gas products and liquid products distributions. (a) TCD channel. (b) FID channel. (c) liquid products analysis.

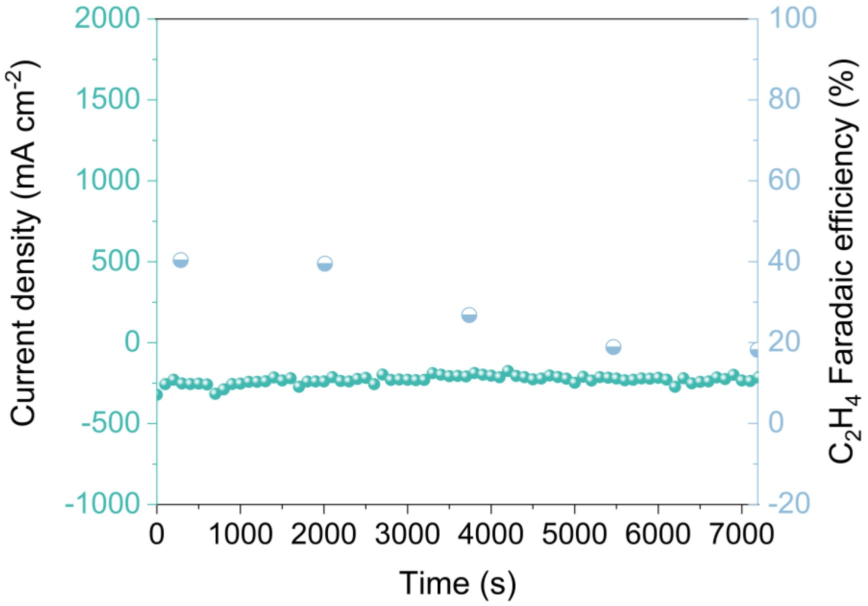

Supplementary Fig. 7. Stability testing of CuNCN. Performance of CuNCN in a three-electrode flow cell to produce ethylene.

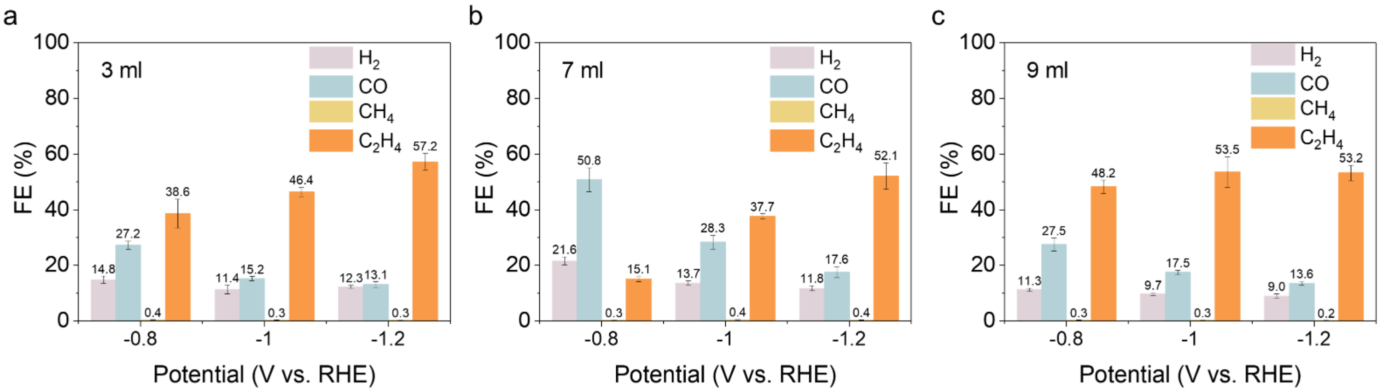

Supplementary Fig. 8. FE of various products of $Cu^{\delta+}$NCN with different levels of reduction at different potentials. (a) Add 3 ml of the reducing agent. (b) Add 7 ml of the reducing agent. (c) Add 9 ml of the reducing agent.

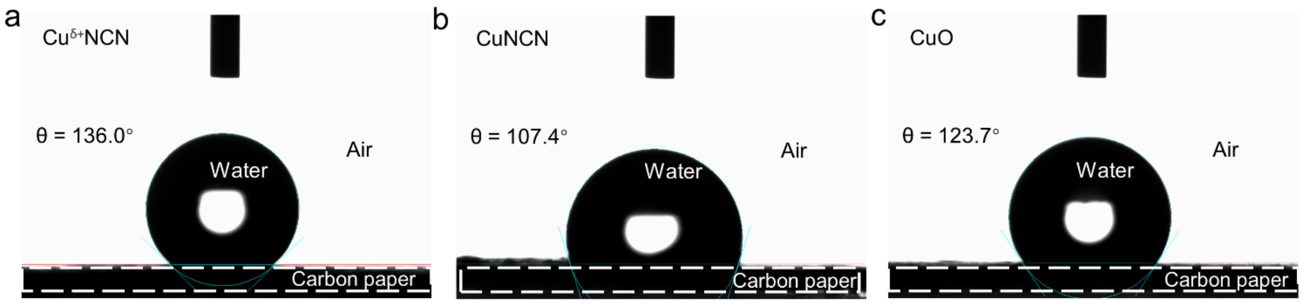

Supplementary Fig. 9. Contact angle measurements for (a) $Cu^{\delta+}NCN$, (b) CuNCN and (c) CuO.

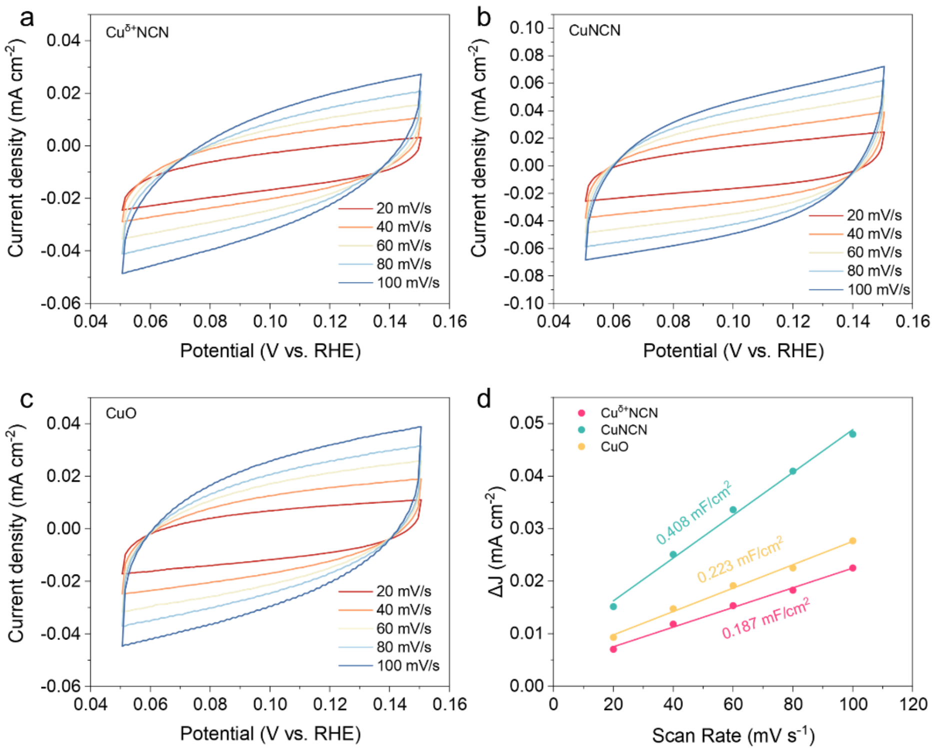

Supplementary Fig. 10. Evaluate the electrochemically active surface area. Cyclic voltammetry curves for (a) Cu$^{\delta+}$NCN, (b) CuNCN, and (c) CuO at varying scan rates, along with (d) the calculated slopes from the fitting of these three samples.

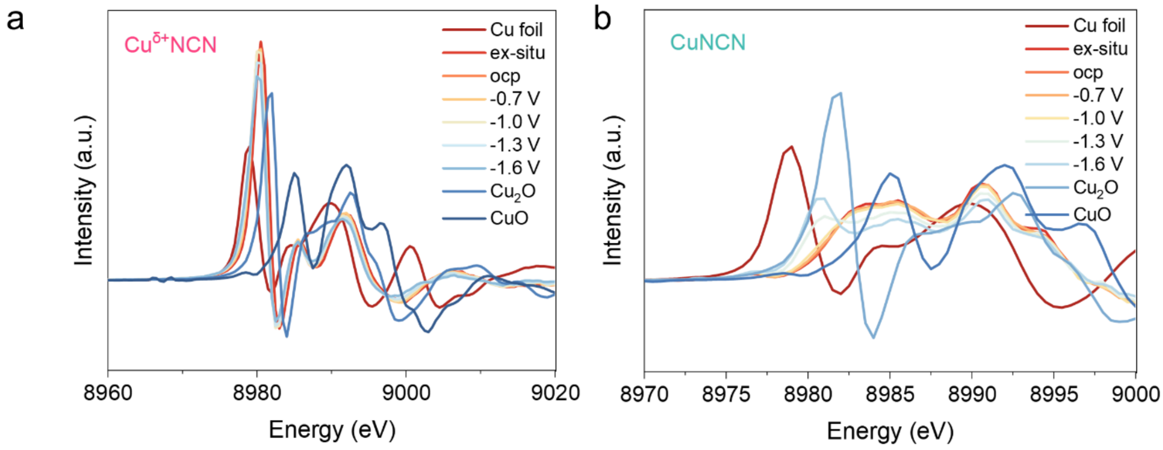

Supplementary Fig. 11. Derived normalized *χμ*(*E*) spectra of (a) Cu$^{\delta+}$NCN and (b) CuNCN in *operando* XANES.

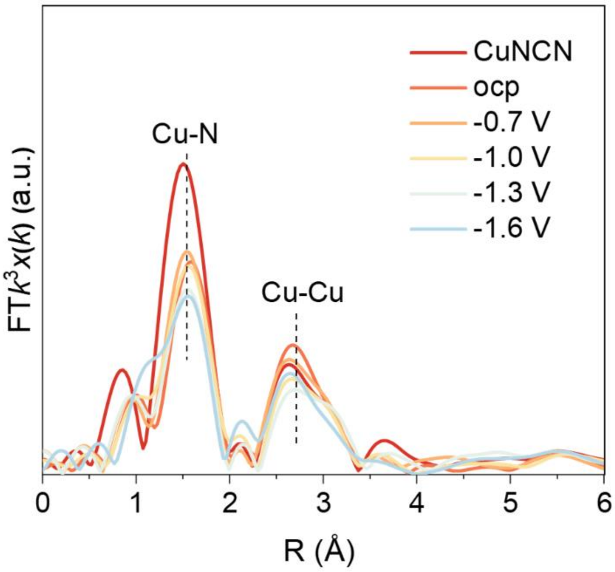

Supplementary Fig. 12. Fourier-transformed k^3-weighted EXAFS signals of the Cu *K*-edge recorded at different potentials for the $Cu^{\delta+}$NCN.

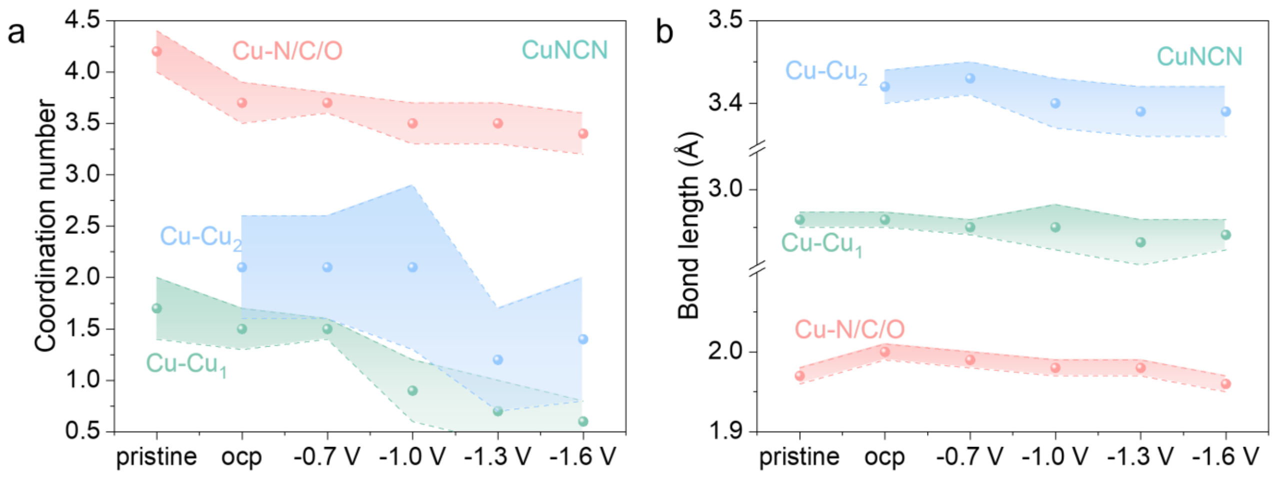

Supplementary Fig. 13. Coordination number and bond length changes of CuNCN during the CO_2RR.

(a) Changes of coordination number for the Cu–N and Cu-Cu coordination shells. (b) Changes of bond length for the Cu–N and Cu-Cu coordination shells.

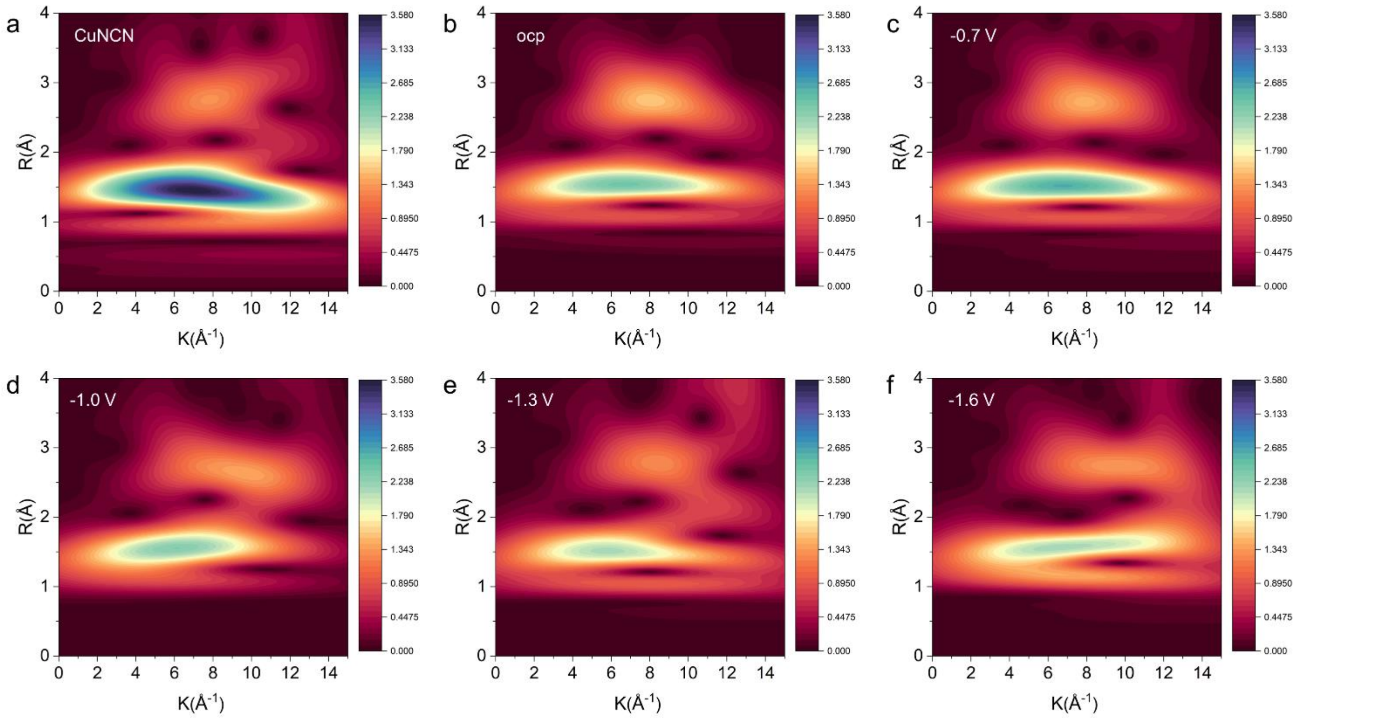

Supplementary Fig. 14. Comparison of the EXAFS WTs of the Cu *K*-edge recorded during *operando* testing of the CuNCN. (a) Initial state. (b) Under open-circuit voltage. (c) At -0.7 V vs. RHE. (d) At -1.0 V vs. RHE. (e) At -1.3 V vs. RHE. (f) At -1.6 V vs. RHE.

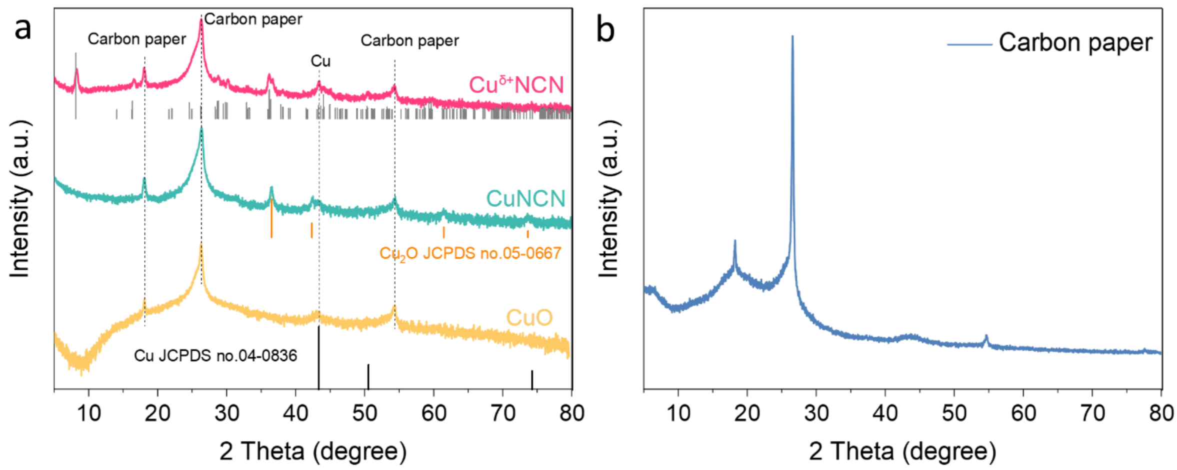

Supplementary Fig. 15. Structure of Cu$^{δ+}$NCN, CuNCN and CuO after the CO_2RR electrolysis. (a) XRD pattern. (b) XRD pattern of the carbon paper used for the test.

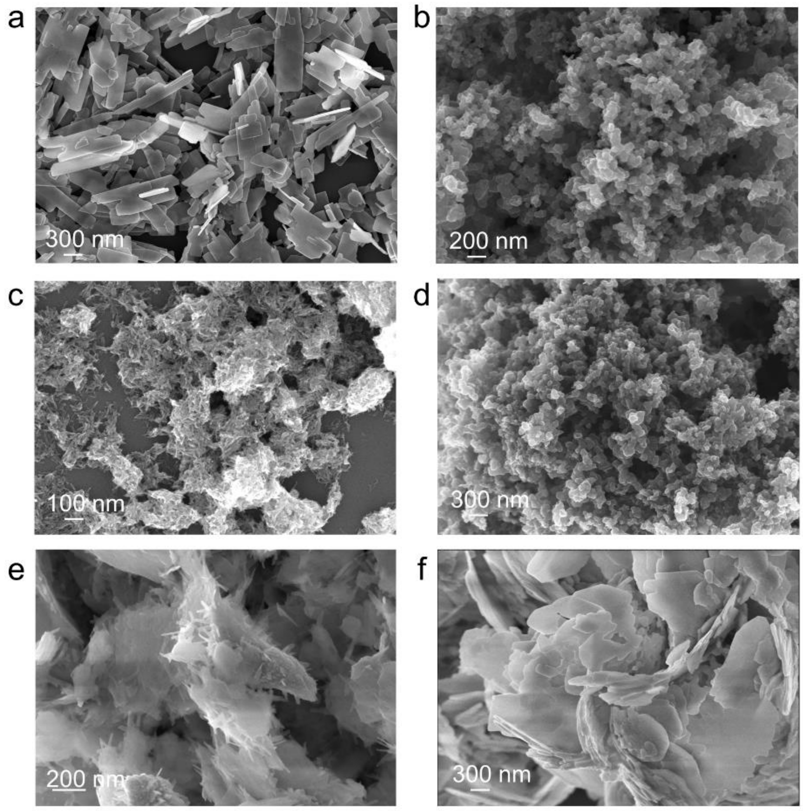

Supplementary Fig. 16. Morphology of $Cu^{\delta+}$NCN, CuNCN and CuO before and after the CO_2RR electrolysis. (a) SEM images of the CuO. (b) SEM images of the CuO after CO_2RR process. (c) SEM images of the CuNCN. (d) SEM images of the CuNCN after CO_2RR process. (e) SEM images of the $Cu^{\delta+}$NCN. (f) SEM images of the $Cu^{\delta+}$NCN after CO_2RR process.

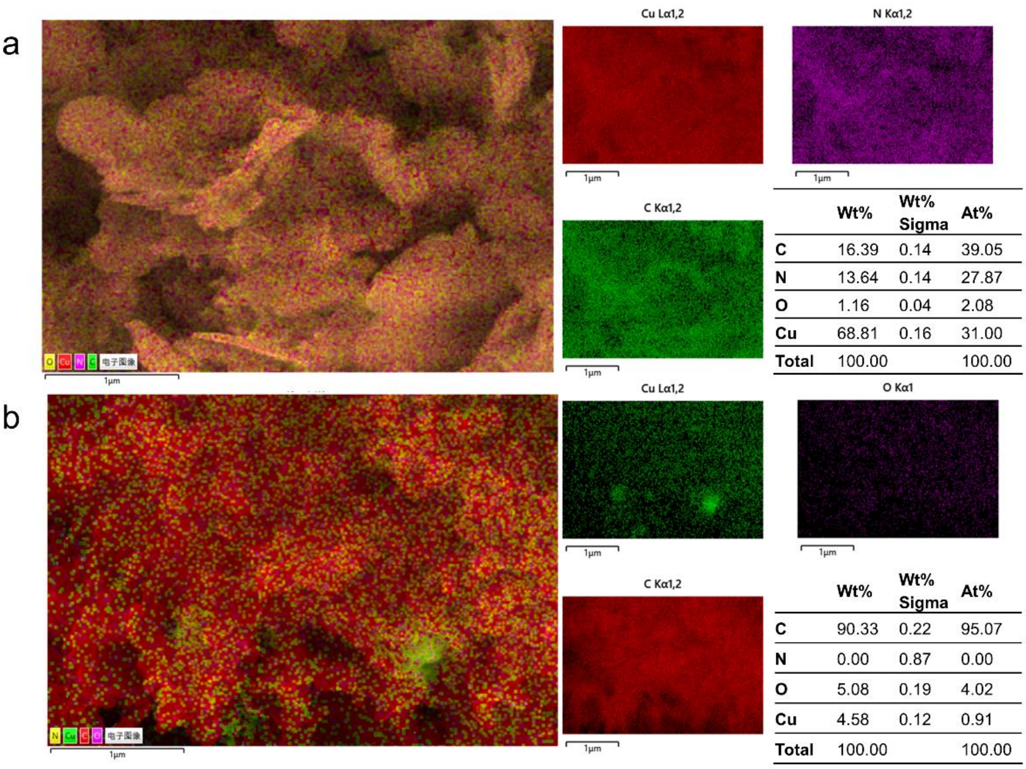

	Wt%	Wt% Sigma	At%
C	16.39	0.14	39.05
N	13.64	0.14	27.87
O	1.16	0.04	2.08
Cu	68.81	0.16	31.00
Total	100.00		100.00

	Wt%	Wt% Sigma	At%
C	90.33	0.22	95.07
N	0.00	0.87	0.00
O	5.08	0.19	4.02
Cu	4.58	0.12	0.91
Total	100.00		100.00

Supplementary Fig. 17. Elemental mapping images and EDX spectra for (a) $Cu^{\delta+}$NCN and (b) CuNCN after CO_2RR process.

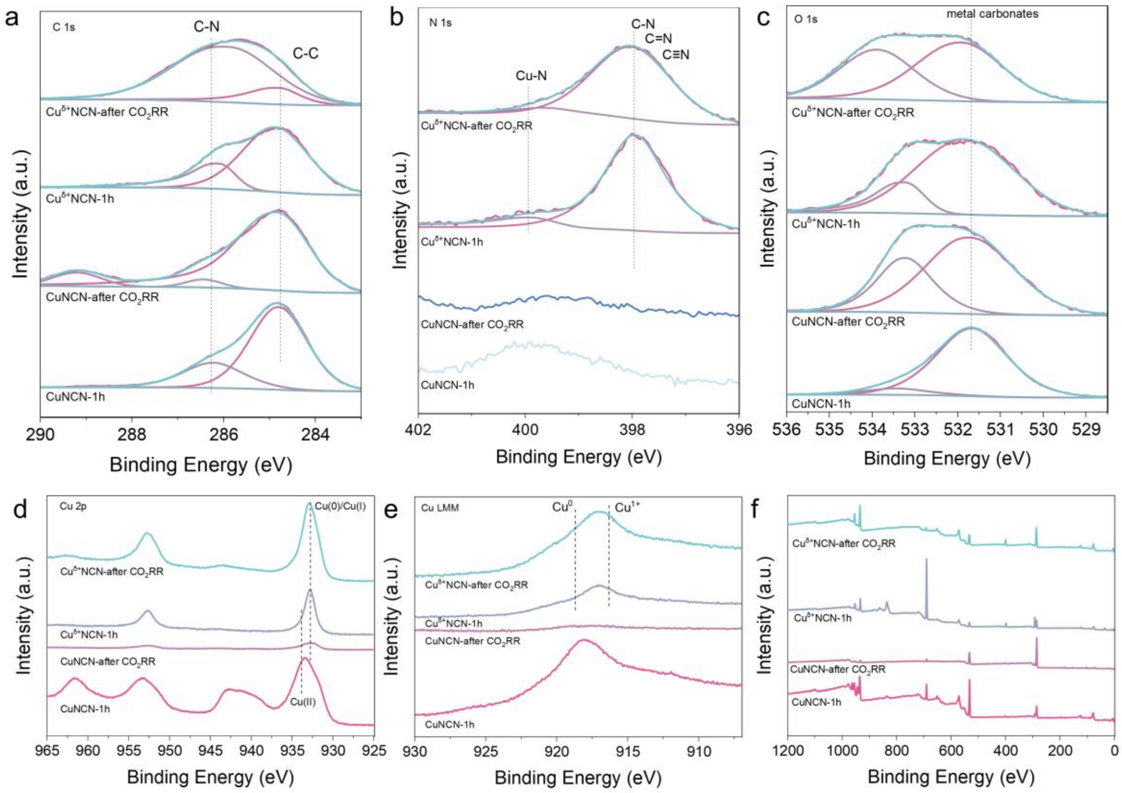

Supplementary Fig. 18. XPS spectra of Cu$^{\delta+}$NCN, and CuNCN after undergoing CO_2RR for 1h and 15h, respectively. (a) C 1s high-resolution XPS. (b) N 1s high-resolution XPS. (c) O 1s high-resolution XPS. (d) Cu 2p high-resolution XPS. (e) Cu LMM spectra. (f) XPS survey spectra.

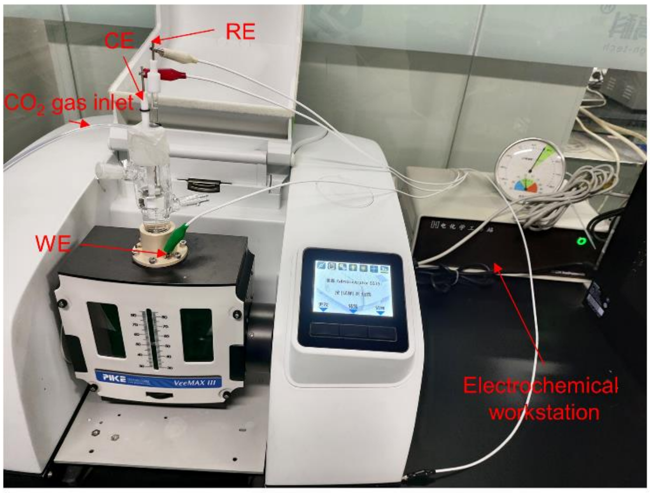

Supplementary Fig. 19. Equipment for *operando* ATR-SEIRA spectra test equipment. The electrolyte used is CO_2-saturated $KHCO_3$**.**

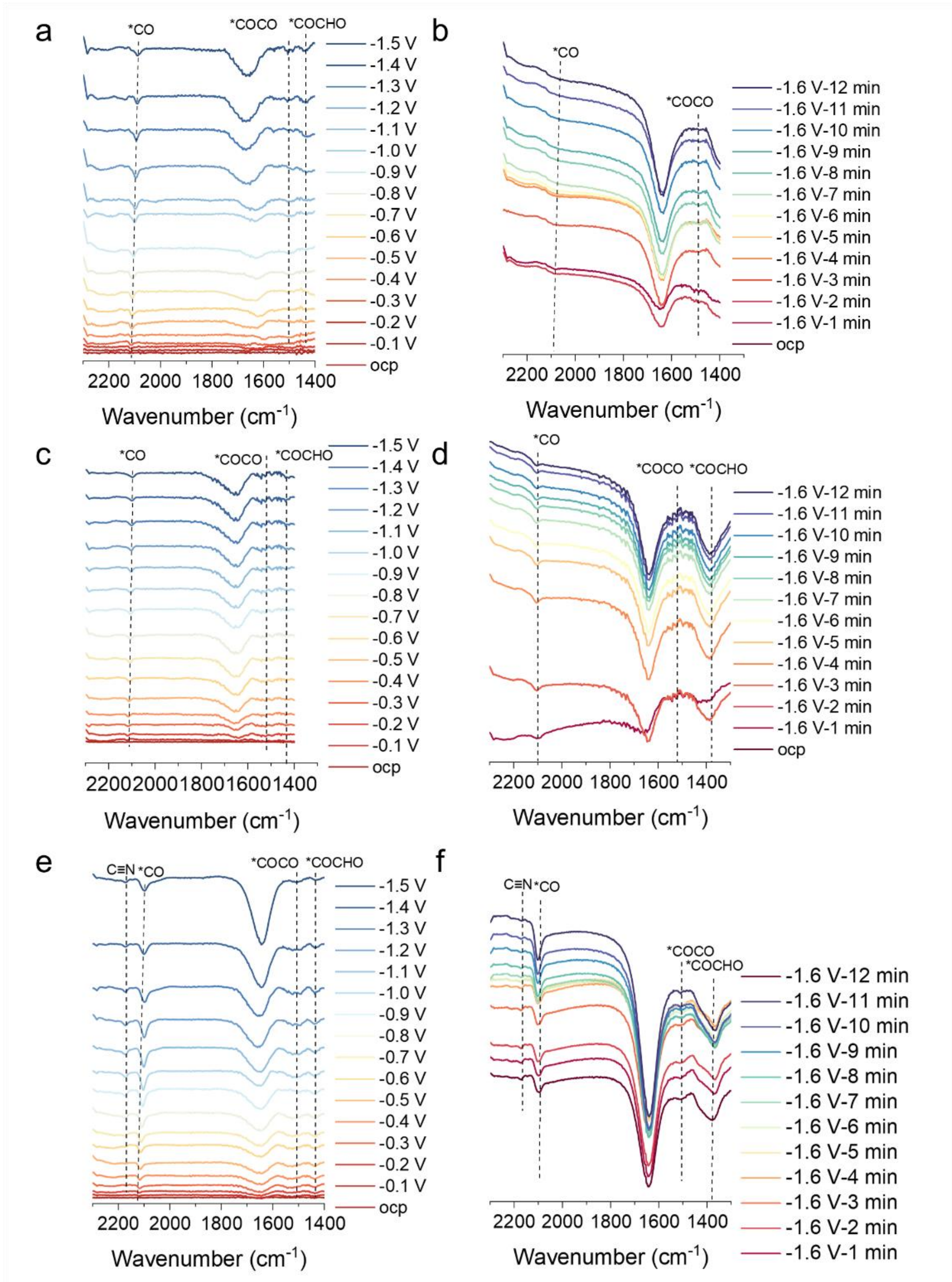

Supplementary Fig. 20. The 2D *operando* ATR-SEIRA spectra of CO_2RR of (a-b) CuO, (c-d) CuNCN, and (e-f) $Cu^{\delta+}$NCN.

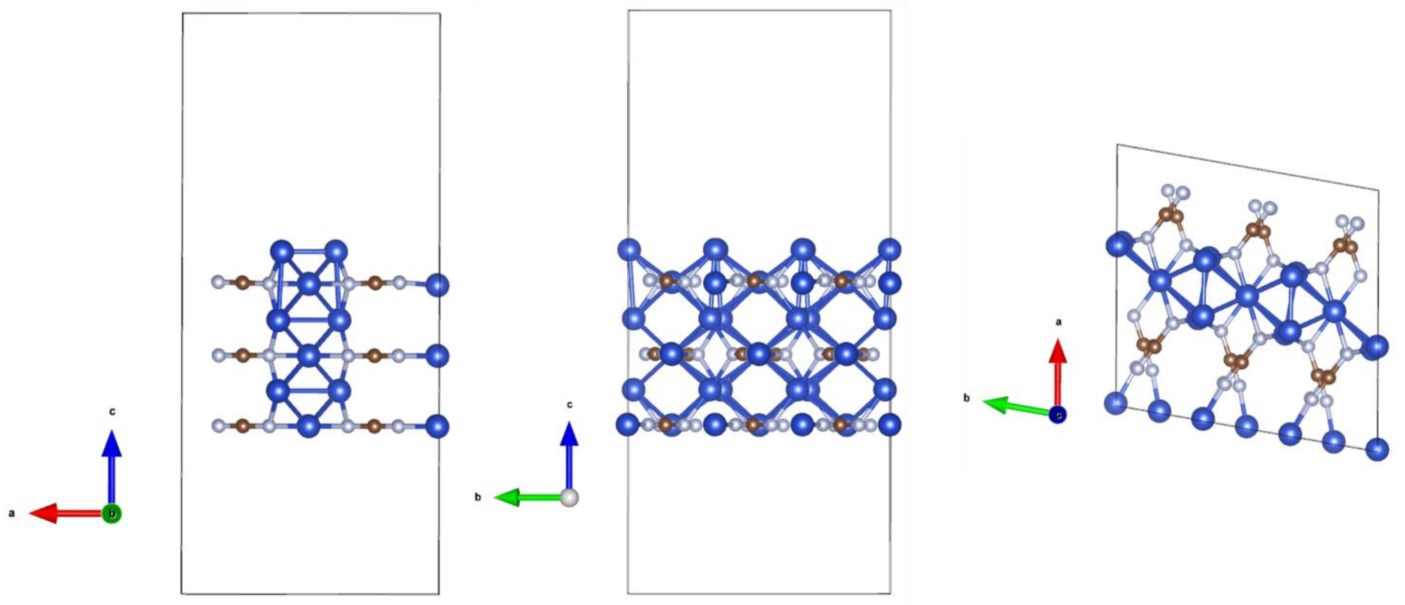

Supplementary Fig. 21. Models of $Cu^{\delta+}$NCN structure. Cu_2NCN coordinated Cu^0-Cu^0 dual atoms model was used to represent the catalytic site

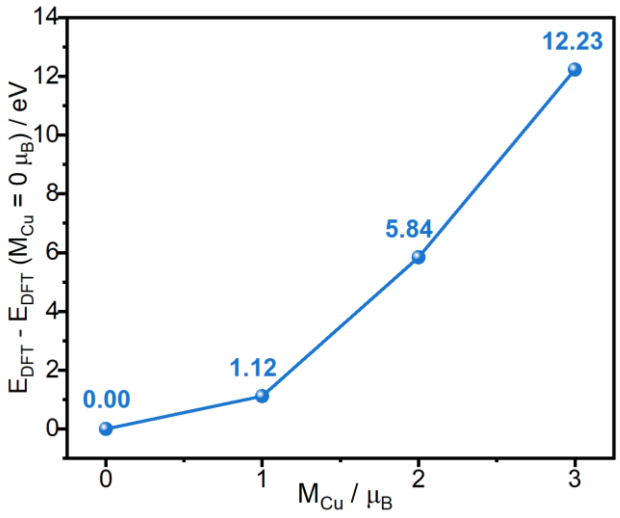

Supplementary Fig. 22. Energy calculations under different magnetic moments. The total energies of the $Cu^{\delta+}NCN$ calculated with different magnetic moments of the Cu^0 atoms (M_{Cu} = 0, 1, 2, and 3 μB).

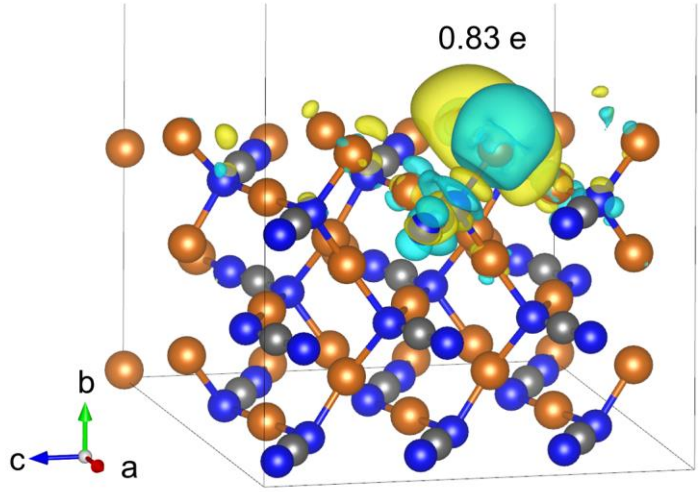

Supplementary Fig. 23. Charge density difference plots. The side views of the three-dimensional charge density difference plots of $Cu^{\delta+}NCN$.

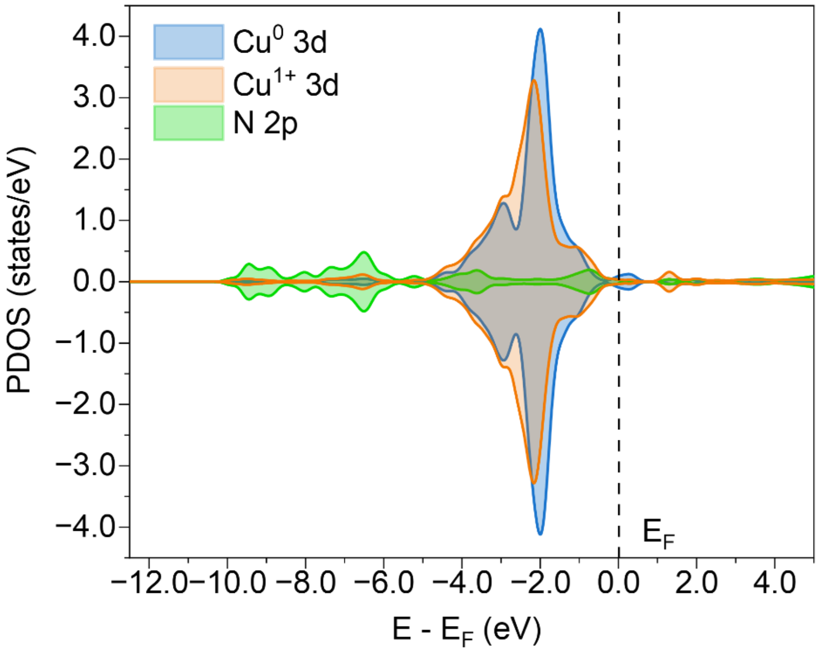

Supplementary Fig. 24. Density of states from DFT calculations. The calculated projected density of states results for $Cu^{\delta+}NCN$.

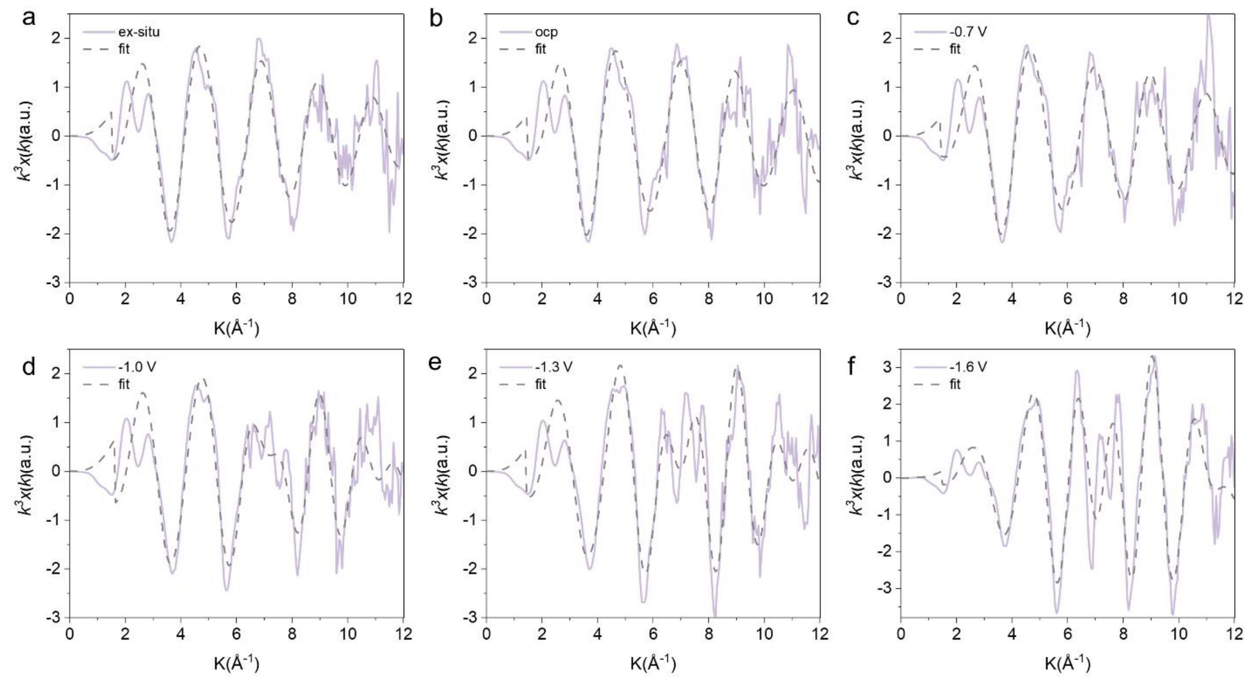

Supplementary Fig. 25. Operando *k*^{3}-weighted Cu *K*-edge EXAFS spectra for Cu$^{\delta+}$NCN under at representative potentials. (a) Initial state. (b) Under open-circuit voltage. (c) At -0.7 V vs. RHE. (d) At -1.0 V vs. RHE. (e) At -1.3 V vs. RHE. (f) At -1.6 V vs. RHE.

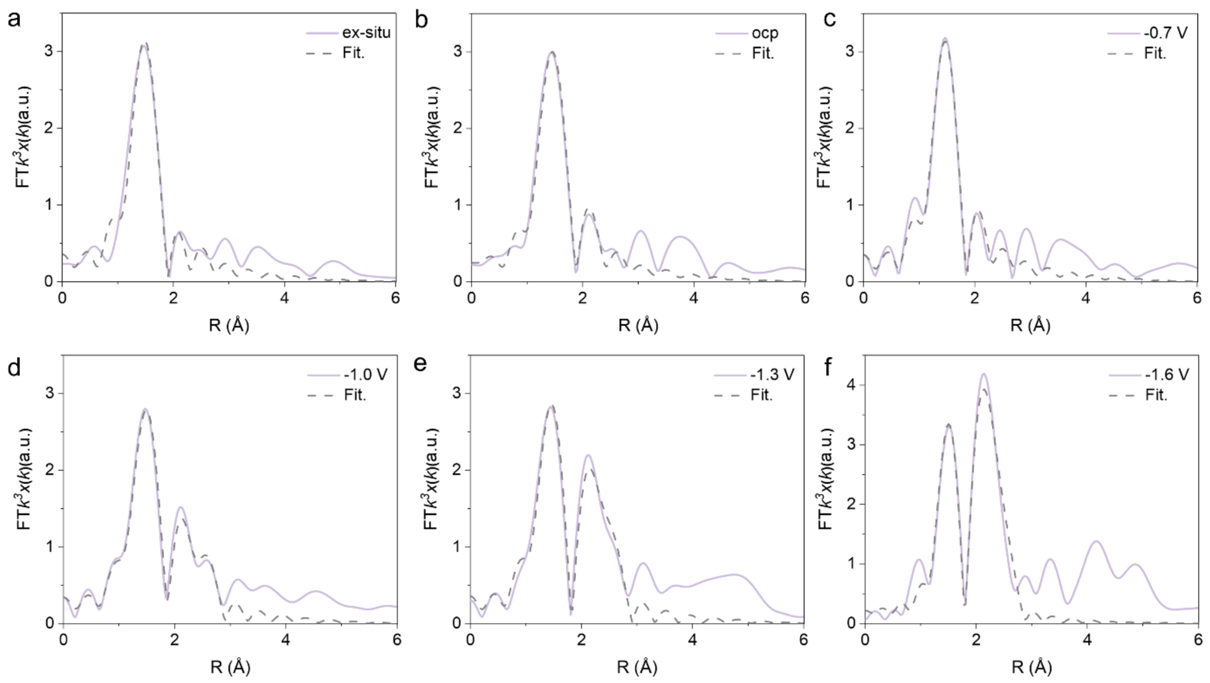

Supplementary Fig. 26. Fourier-transformed magnitudes for $Cu^{\delta+}$NCN under at representative potentials. (a) Initial state. (b) Under open-circuit voltage. (c) At -0.7 V vs. RHE. (d) At -1.0 V vs. RHE. (e) At -1.3 V vs. RHE. (f) At -1.6 V vs. RHE.

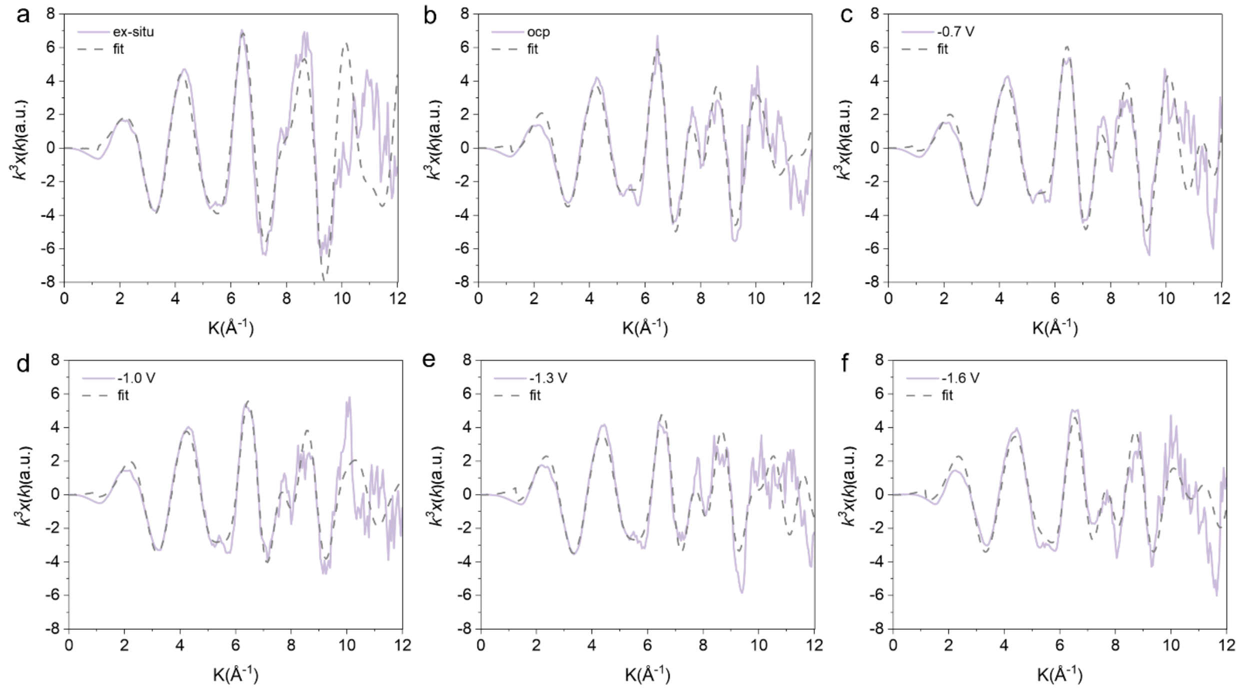

Supplementary Fig. 27. Operando k^3-weighted Cu *K*-edge EXAFS spectra for CuNCN under at representative potentials. (a) Initial state. (b) Under open-circuit voltage. (c) At -0.7 V vs. RHE. (d) At -1.0 V vs. RHE. (e) At -1.3 V vs. RHE. (f) At -1.6 V vs. RHE.

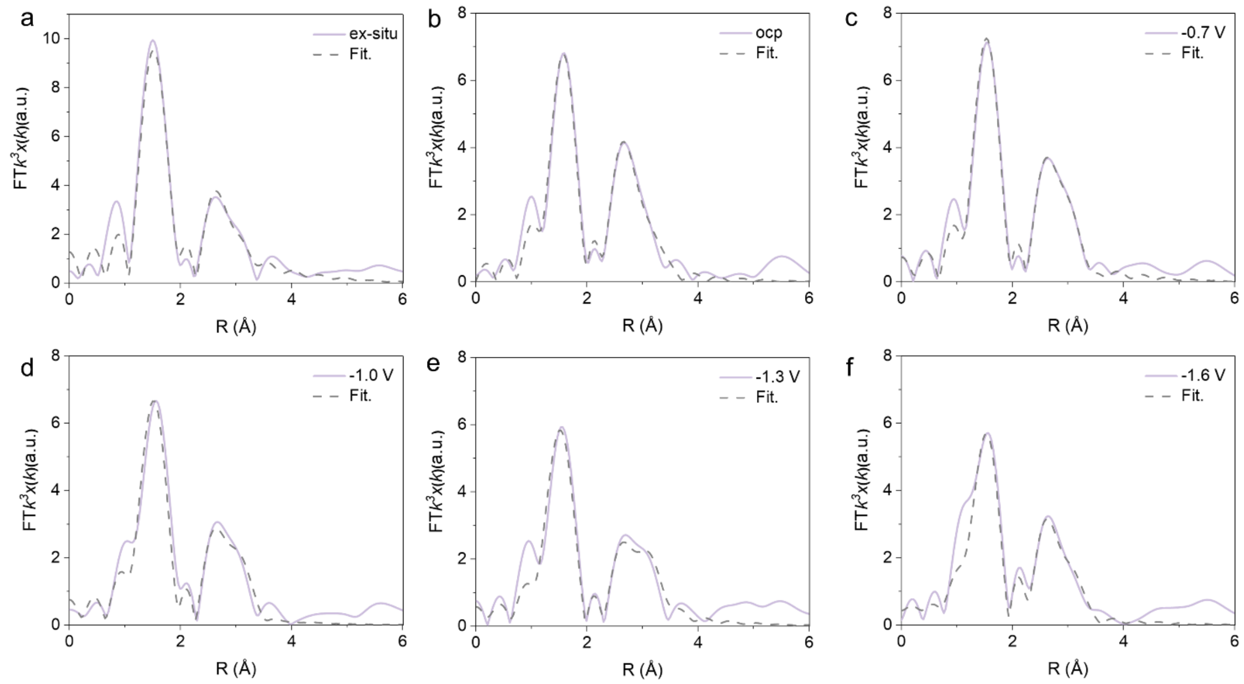

Supplementary Fig. 28. Fourier-transformed magnitudes for CuNCN under at representative potentials. (a) Initial state. (b) Under open-circuit voltage. (c) At -0.7 V vs. RHE. (d) At -1.0 V vs. RHE. (e) At -1.3 V vs. RHE. (f) At -1.6 V vs. RHE.

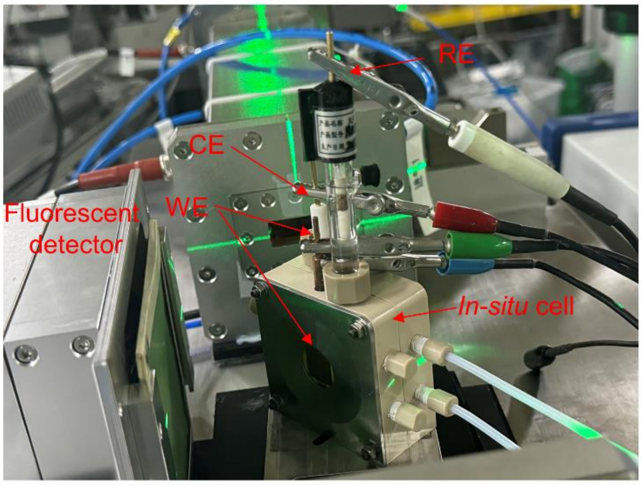

Supplementary Fig. 29. $Cu^{\delta+}$NCN and CuNCN in the *operando* XAFS testing environment for Cu *K*-edge spectra of catalysis (test beamline station is the SSRF BL17B1).

Supplementary Table 1. ICP-OES of the atom ratio in CuNCN and $Cu^{\delta+}$NCN.

Samples	Cu (%)
CuNCN	60.45%
$Cu^{\delta+}$NCN	67.23%

Supplementary Table 2. EXAFS fitting parameters for the Cu *K*-edge of the $Cu^{\delta+}NCN$ (S_0^2=0.83)

	shell	CN	R(Å)	σ^2	ΔE_0	R factor
Cu foil	Cu-Cu	12*	2.54±0.01	0.0086	4.2±0.5	0.0040
ex-situ	Cu-N/C/O	1.6±0.1	1.89±0.01	0.0043	8.7±0.9	0.0113
Cu-ocp	Cu-N/C/O	1.4±0.1	1.88±0.01	0.0028	8.2±1.0	0.0069
	Cu-C	0.7±0.3	2.65±0.04	0.0032		
-0.7 V	Cu-N/C/O	1.4±0.1	1.88±0.01	0.0030	8.0±0.9	0.0067
	Cu-C	0.9±0.3	2.63±0.04	0.0088		
-1.0 V	Cu-N/C/O	1.7±0.1	1.90±0.01	0.0065	9.9±1.2	0.0098
	Cu-Cu	0.5±0.1	2.58±0.02	0.0056		
-1.3 V	Cu-N/C/O	1.6±0.1	1.87±0.02	0.0054	7.9±1.7	0.0177
	Cu-Cu	0.9±0.2	2.58±0.02	0.0071		
-1.6 V	Cu-N/C/O	1.1±0.1	1.88±0.01	0.0010	8.2±1.5	0.0131
	Cu-Cu	1.6±0.2	2.57±0.01	0.0085		
	Cu-N/C/O	1.4±0.3	2.52±0.03	0.0037		

[a]*N*: coordination numbers; [b]*R*: bond distance; [c]σ^2: Debye-Waller factors; [d] ΔE_0: the inner potential correction. *R* factor: goodness of fit.

Supplementary Table 3. EXAFS fitting parameters for the Cu *K*-edge of the CuNCN (S_0^2=0.83)

	shell	CN	R(Å)	σ^2	ΔE_0	R factor
Cu foil	Cu-Cu	12*	2.54±0.01	0.0086	4.2±0.5	0.0040
ex-situ	Cu-N/C/O	4.2±0.2	1.97±0.01	0.0001	5.9±0.8	0.0103
	Cu-Cu1	1.7±0.3	2.96±0.01	0.0033		
Cu-ocp	Cu-N/C/O	3.7±0.2	2.00±0.01	0.0031	5.2±0.9	0.0081
	Cu-Cu1	1.5±0.2	2.96±0.01	0.0045		
	Cu-Cu2	2.1±0.5	3.42±0.02	0.0085		
-0.7 V	Cu-N/C/O	3.7±0.1	1.99±0.01	0.0023	3.9±0.6	0.0055
	Cu-Cu1	1.5±0.1	2.95±0.01	0.0001		
	Cu-Cu2	2.1±0.5	3.43±0.02	0.0081		
-1.0 V	Cu-N/C/O	3.5±0.2	1.98±0.01	0.0035	3.0±1.0	0.0171
	Cu-Cu1	0.9±0.3	2.95±0.03	0.0083		
	Cu-Cu2	2.1±0.8	3.40±0.03	0.0081		
-1.3 V	Cu-N/C/O	3.5±0.2	1.98±0.01	0.0045	6.0±1.1	0.0171
	Cu-Cu1	0.7±0.3	2.93±0.03	0.0026		
	Cu-Cu2	1.2±0.5	3.39±0.03	0.0001		
-1.6 V	Cu-N/C/O	3.4±0.2	1.96±0.01	0.0055	5.4±1.2	0.0114
	Cu-Cu1	0.6±0.2	2.94±0.02	0.0001		
	Cu-Cu2	1.4±0.6	3.39±0.03	0.0070		

[a]*N*: coordination numbers; [b]*R*: bond distance; [c]σ^2: Debye-Waller factors; [d] ΔE_0: the inner potential correction. *R* factor: goodness of fit.

Supplementary Table 4. Performance comparison of state-of-the-art catalysts for CO_2RR to C_2H_4 reported in the literature.

Catalyst	Potential (V vs. RHE)	FE (%)	Current density ($mA\ cm^{-2}$)	Stability (h)	Reference
$Cu^{\delta+}NCN$	-1.4	77.7	400	15	This work
	3.6*	66.8	180	78	
Cu	4.2*	25	1200	12	Science 2021, 372, 1074
Cu-Al	~-1.7	75±4	400	100	Nature 2020, 581, 178
Cu-P1	-0.99	72	400	/	Nat Catal., 2021, 4, 20
A-CuNWs	-1.0±0.01	~77.4	17.3	200	Nat. Catal., 2020, 3, 804
F-Cu	~-0.6	80	320	40	Nat. Catal. 2020, 3, 478–487
cAA-CuNW	-1.27	60.7	539	/	Nat Commun. 2024, 15, 192
CuPO	~-1.7	~48	300	18	Nat.Commun.,2023, 14, 7681
Ni SAC+Cu-R	-1.4	60	500	14	J. Am. Chem. Soc. 2024, 146, 468
PcCu-Cu-O	~-1.2	50	7.3	4	J. Am. Chem. Soc. 2021, 143, 7242
GB-Cu	-1.2	40	~52	3	J. Am. Chem. Soc. 2020, 142, 6878
Cu-S motifs	~-1.2	~50	150	8	Angew. Chem. Int. Ed. 2022, 61, e202111700
Cu_{3-X}	-0.7	55.01	129.58	9	Angew. Chem. Int. Ed.2021, 60, 26210
TA-Cu	3.35*	50	500_{total}	10	Angew. Chem. 2023, 135, e202315621
Mg-Cu	~-0.75	70	455	48	Angew. Chem. Int. Ed. 2022, 61, e202213423

* Represents the electrolyser voltage in the MEA system.

Supplementary Table 5. Reaction paths of the intermediates involved in the reaction at U = -0.8 V and reaction energies, with the corresponding kinetic potentials for the key reaction steps in parentheses

Reactive species	Reaction process	Reaction products	Free energy change
*(sub)	$+CO_2$	$*CO_2$	0.23
$*CO_2$	$+2(H^+ + e^-)-H_2O$	*CO	-1.68
*CO	$+CO_2+2(H^+ + e^-)-H_2O$	2*CO	-0.96
2*CO	*CO dimerization	*COCO	-0.01 (0.86)
*COCO	$+ H^+ + e^-$	*COCOH	-1.28
		*COCHO	-1.45
*COCHO	$+3(H^+ + e^-)-H_2O$	*CHCOH	-3.80
*CHCOH	$+ H^+ + e^-$	*CHCHOH	-0.68 (1.07)
	$+ H^+ + e^- - H_2O$	*CHC	-1.02 (0.64)

Supplementary Table 6. The crystallographic information file (.CIF) for $Cu^{\delta+}NCN$ sample.

data_ $Cu^{\delta+}NCN$ -surface:
_cell_length_a 11.2339
_cell_length_b 11.4027
_cell_length_c 25
_cell_angle_alpha 90.002
_cell_angle_beta 90.0007
_cell_angle_gamma 80.2593
loop_
_symmetry_equiv_pos_as_xyz
+x,+y,+z
loop_
_atom_site_type_symbol
_atom_site_label
_atom_site_fract_x
_atom_site_fract_y
_atom_site_fract_z

C	C	0.76270308	0.81000504	0.28933427
C	C	0.76270308	0.47667171	0.28933427
C	C	0.76270308	0.14333838	0.28933427
C	C	0.25208284	0.19003512	0.28933615
C	C	0.25208284	0.85670178	0.28933615
C	C	0.25208284	0.52336845	0.28933615
C	C	0.25193203	0.89587968	0.41066943
C	C	0.25193203	0.22921301	0.41066943
C	C	0.25193203	0.56254635	0.41066943
C	C	0.76285392	0.10416404	0.41067166
C	C	0.76285392	0.77083071	0.41067166
C	C	0.76285392	0.43749737	0.41067166
C	C	0.76497885	0.48019893	0.53580721
C	C	0.76497887	0.81348673	0.53580606
C	C	0.76498147	0.14685214	0.53581973
C	C	0.24981291	0.18657136	0.53580292
C	C	0.24980690	0.85322201	0.53581669
C	C	0.24982101	0.51983759	0.53580815
N	N	0.66038462	0.88101430	0.28933399
N	N	0.66038462	0.54768097	0.28933399
N	N	0.66038462	0.21434764	0.28933399
N	N	0.85619565	0.41099891	0.28933497
N	N	0.85619565	0.74433224	0.28933497
N	N	0.85619565	0.07766557	0.28933497
N	N	0.15858489	0.25569938	0.28933546
N	N	0.15858489	0.58903272	0.28933546
N	N	0.15858489	0.92236605	0.28933546
N	N	0.35440207	0.11902761	0.28933643

N	N	0.35440207	0.78569428	0.28933643
N	N	0.35440207	0.45236095	0.28933643
N	N	0.35448101	0.59905507	0.41066942
N	N	0.35448101	0.93238840	0.41066942
N	N	0.35448101	0.26572173	0.41066942
N	N	0.15818609	0.19525018	0.41067028
N	N	0.15818609	0.86191685	0.41067028
N	N	0.15818609	0.52858352	0.41067028
N	N	0.85659371	0.47147126	0.41067080
N	N	0.85659371	0.80480460	0.41067080
N	N	0.85659371	0.13813793	0.41067080
N	N	0.66030559	0.06765255	0.41067165
N	N	0.66030559	0.40098588	0.41067165
N	N	0.66030559	0.73431922	0.41067165
N	N	0.66245762	0.55006573	0.53428640
N	N	0.66246356	0.21672361	0.53430415
N	N	0.66244320	0.88335102	0.53429992
N	N	0.85952235	0.41602107	0.53688867
N	N	0.85953037	0.74932662	0.53687600
N	N	0.85951572	0.08267098	0.53690924
N	N	0.15527001	0.25074205	0.53687522
N	N	0.15526686	0.91740098	0.53690136
N	N	0.15527240	0.58399987	0.53688752
N	N	0.35233251	0.11670304	0.53429238
N	N	0.35233858	0.44997149	0.53429210
N	N	0.35231279	0.78332450	0.53429964
Cu	Cu	0.50739408	0.83335250	0.28933520
Cu	Cu	0.50739408	0.50001917	0.28933520
Cu	Cu	0.50739408	0.16668584	0.28933520
Cu	Cu	0.00738963	0.00001698	0.28933523
Cu	Cu	0.00738963	0.66668364	0.28933523
Cu	Cu	0.00738963	0.33335031	0.28933523
Cu	Cu	0.38808049	0.68681159	0.35000834
Cu	Cu	0.38808049	0.35347826	0.35000834
Cu	Cu	0.38808049	0.02014493	0.35000834
Cu	Cu	0.62671314	0.31322903	0.35000836
Cu	Cu	0.62671314	0.64656237	0.35000836
Cu	Cu	0.62671314	0.97989570	0.35000836
Cu	Cu	0.00738948	0.50002605	0.41067052
Cu	Cu	0.00738948	0.83335938	0.41067052
Cu	Cu	0.00738948	0.16669272	0.41067052
Cu	Cu	0.50739414	0.50002200	0.41067055
Cu	Cu	0.50739414	0.16668867	0.41067055
Cu	Cu	0.50739414	0.83335534	0.41067055
Cu	Cu	0.62643201	0.64631576	0.47194993
Cu	Cu	0.62645210	0.31299845	0.47195974
Cu	Cu	0.62646471	0.97963652	0.47195568

Cu	Cu	0.38834667	0.02041064	0.47195071
Cu	Cu	0.38833437	0.68703164	0.47195720
Cu	Cu	0.38836104	0.35373246	0.47194792
Cu	Cu	0.50736731	0.83333665	0.53412241
Cu	Cu	0.50739928	0.50001096	0.53410469
Cu	Cu	0.50740329	0.16669763	0.53411126
Cu	Cu	0.00738277	0.00003487	0.53189682
Cu	Cu	0.00741344	0.66665125	0.53188125
Cu	Cu	0.00741063	0.33340002	0.53187367
Cu	Cu	0.40212808	0.33627201	0.58972725
Cu	Cu	0.40206599	0.66955893	0.58969650
Cu	Cu	0.40207584	0.00292961	0.58968817
Cu	Cu	0.61272646	0.33048898	0.58972441
Cu	Cu	0.61270882	0.99711956	0.58969732
Cu	Cu	0.61268631	0.66375833	0.58970980